ACS APPLIED MATERIALS & INTERFACES

Research Article

Cite This: ACS Appl. Mater. Interfaces 2019, 11, 1563−1570

www.acsami.org

Engineering Surface Patterns with Shape Memory Polymers: Multiple Design Dimensions for Diverse and Hierarchical Structures

Lingyu Zhao,[†,‡,§] Liangpei Zhang,[†,∥] Jun Zhao,[*,†,§] Jidong Shi,[†,§] Zhaohe Dai,[⊥] Guorui Wang,[†] Cheng Zhang,[#] Bo Li,[#] Xiqiao Feng,[#] Hui Zhang,[†] Jin Zhang,[‡] and Zhong Zhang[*,†,§]

[†]CAS Key Laboratory of Nanosystem and Hierarchical Fabrication and CAS Center for Excellence in Nanoscience, National Center for Nanoscience and Technology, Beijing 100190, China

[‡]Academy for Advanced Interdisciplinary Studies, Peking University, Beijing 100871, China

[§]University of Chinese Academy of Sciences, Beijing 100049, China

[∥]School of Materials Science and Technology, China University of Geosciences (Beijing), Beijing 100083, China

[⊥]Center for Mechanics of Solids, Structures and Materials, Department of Aerospace Engineering and Engineering Mechanics, The University of Texas at Austin, Austin, Texas 78712, United States

[#]Institute of Biomechanics and Medical Engineering, AML, Department of Engineering Mechanics, Tsinghua University, Beijing, 100084, China

Supporting Information

ABSTRACT: Deterministic design of surface patterns has seen a surge of interests because of their wide applications in flexible and stretchable electronics, microfluidics, and optical devices. Recently, instability of bilayer systems has been extensively utilized by which micro-/nano-patterns of a film can be easily achieved through macroscopically deforming the underlying substrate. For a bilayer system with traditional thermostable substrates, the pattern morphology is only determined by initial strain mismatch of the two layers, and the realization of localized patterns appears to be particularly challenging because of the difficulties associated with manipulating inhomogeneous deformations. In this work, we exploit cross-linked polyethylene (*c*PE), a shape memory polymer (SMP), as the flexible substrate for building micro-/nano-structures of sputtered gold films. We find that the shape memory effect can offer new dimensions for designing diverse and hierarchical surface structures by harnessing film thickness orheating time and by globally or locally controlling the thermal field. By combining those strategies, we further demonstrate versatile hierarchical, superimposed, and local surface patterns based on this *c*PE/gold (Au) system. Piezoresistive pressure sensors are assembled with the obtained patterned surface, which have high sensitivity, operational range, and cyclic stability. These results highlight the unique advantages of SMPs for building arbitrary surface patterns.

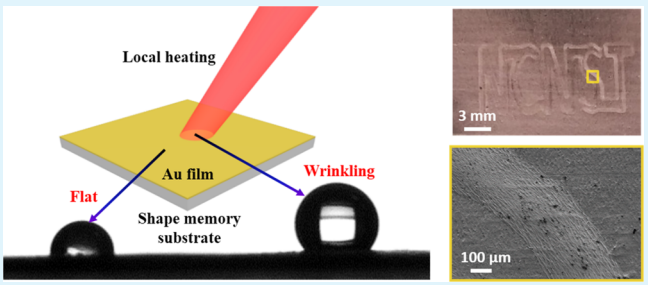

KEYWORDS: *wrinkle, hierarchical structures, local patterning, shape memory polymer, piezoresistive pressure sensor*

INTRODUCTION

Hierarchical surfaces with micro- and nano-scale patterns are ubiquitous in biological species. With unique physical and chemical properties, these surfaces are essential for the survival and daily activities of living organisms.[1,2] For instance, lotus leaves demonstrate superior hydrophobicity and self-cleaning capability with microscale papillae and nanoscale tomenta;[3] geckos could reversibly adhere onto a smooth surface with millions of setae on their feet.[4] Inspired by the delicate natural surfaces, synthetic patterned surfaces with unique optical,[5] electrical,[6] mechanical,[7] and surface wetting properties[8−10] are prepared, which have a variety of applications including microfluidics,[11] optical devices,[12] as well as flexible and stretchable electronics.[13−15] Well-developed lithography techniques have been applied for building exquisite surface patterns with submicron resolution,[16,17] while lithography process is usually costly and time-consuming. Recently, surface patterning by utilizing the instability of bilayer systems has been adopted, by which out-of-plane wrinkling of stiff films was activated by applying a compressive strain to the underlying substrate, usually through utilizing the thermal expansion mismatch between the film and substrate[18,19] or prestretching the substrate followed by film transfer and prestrain release.[20,21] This strain engineering methodology offers unprecedented scalability through manipulating microscopic structural evolution in a macroscopic way. While these studies

Received: September 6, 2018
Accepted: November 30, 2018
Published: November 30, 2018

DOI: 10.1021/acsami.8b15535
ACS Appl. Mater. Interfaces 2019, 11, 1563−1570

have substantially advanced state-of-the-art surface designs, it remains an open question how to achieve hierarchically patterned surfaces in a low-cost, scalable, and more importantly, controllable manner for broad industrial applications.

Traditional substrates for building the bilayer system are usually thermostable elastomers, such as polydimethylsiloxane[22−25] and polyethylene terephthalate.[26] In contrast, shape memory polymers (SMPs) are one kind of smart materials that could maintain the temporary deformation and recover to their thermodynamically stable shape upon exposure to an external stimulus such as heat, light, electric field, and pH change.[27−31] Taking the example of heat-induced shape recovery process, the degree of shape recovery is correlated to both the recovery temperature and time, and the shape of partially recovered SMP could be fixed by quick cooling below switch temperature (T_{sw}), allowing for various shape control of SMPs.[32−34] SMPs could also serve as the substrate in a bilayer system, which could be further applied in the preparation of surface wrinkles. Therefore, instead of mere mechanical loadings, the heat-driven deformation of SMPs provides a controlled, precise way to deform the substrate in above-mentioned bilayer systems.[35−42] For example, Khine et al. deposited a 10 nm Au film onto a prestretched shape memory polystyrene (PS) substrate, and achieved both uniaxial and biaxial patterns through the release of prestrain, which was applied for the enhancement of fluorescent intensity.[35] Wong et al. prepared a multiscale graphene surface through sequential shape recovery of the PS substrate, which had ultrahigh hydrophobicity and charge storage capacity.[42] Significantly, the shape recovery process was activated by bond rupture and rebuilding within SMPs at elevated temperature, which could be spatially confined for the preparation of localized patterns. Xie et al. applied a normal pressure onto an epoxy-based SMP before the deposition of the Au/Pd film.[43] Lateral compression could be produced after the temperature was increased above T_{sw}, rendering a localized shape recovery, and thus, the wrinkle formation. Nam et al. also prepared localized wrinkles through spatially selective heating of an SMP substrate.[44] The capability for local patterning endows SMPs great superiority for surface patterning in bilayer systems, compared with traditional thermostable substrates. Despite the great advancements, a controlled preparation of hierarchical surface patterns in SMP-based bilayer system is still lacking.

Herein, we prepared a bilayer system by sputtering Au film onto a prestretched shape memory cross-linked polyethylene (*c*PE) substrate. The morphological evolution of surface patterns was first investigated through tuning the shape recovery temperature and time of *c*PE, as well as the thickness of the sputtered Au film. Versatile complex surface patterns could be prepared in this Au/*c*PE system. Superimposed hierarchical patterns could be prepared by a two-step sequential shape recovery of *c*PE and prepatterning the Au film using a shadow mask. Besides, the surface patterns could be localized in the defined area through laser-induced local heating, which was further extended for "writing" an arbitrary trajectory composed of wrinkles. The as-prepared patterned surface was applied for constructing piezoresistive pressure sensors, with high sensitivity, operational range, and cyclic stability, which is seldom reported in previous publications and shows great promise in electronical-skin applications. In all, the surface patterning methodology with our Au/*c*PE bilayer system could provide significant theoretical and technical guidance in the controlled preparation of versatile hierarchical surface structures.

RESULTS AND DISCUSSIONS

*c*PE, an SMP with appropriately low T_{sw} of ca. 105 °C[45−47] (Figure S1a,b in the Supporting Information) and a deformable strain of up to ca. 205% at 110 °C (Figure S1c in the Supporting Information) is chosen as the substrate for building the bilayer system. *c*PE has a strong shape memory effect, with both the strain fixity ratio and strain recovery ratio above 90%, as shown in Figure S1d in the Supporting Information. The schematic for the preparation of microscale uniaxial patterns is shown in Figure 1a. The *c*PE substrate is

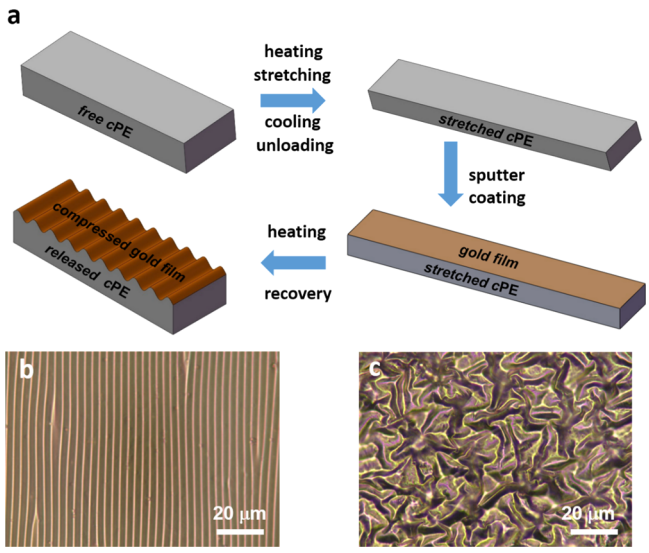

Figure 1. Preparation of surface patterns based on the recovery of *c*PE SMP substrates. (a) Schematic of the pattern preparation process. (b) Optical image of typical wave-like buckled structures. (c) Optical image of random crumpled structures. Gold film for (b,c) is ca. 15.0 nm in thickness.

first heated to ca. 110.0 °C before a tensile strain is applied. The prestretched *c*PE substrate is then quickly cooled down to room temperature of ca. 25.0 °C to fix the deformation. After the removal of the external force, a layer of Au film is sputtered onto the *c*PE substrate, with the thickness determined by the sputtering time (Figure S2 in the Supporting Information). The as-prepared bilayer system is then heated again above T_{sw} of *c*PE for the shape recovery process, with the equivalent compressive strain tuned by recovery temperature and time (Figure S3 in the Supporting Information). The compressive strain could be transferred to Au film through the interfacial shear stress and induce the out-of-plane wrinkling of the film. The patterns could be fixed by ceasing the shape recovery process through quickly cooling down the bilayer system. As shown in Figure 1b,c, periodic wave-like buckles and quasirandom surface crumples could be obtained by releasing the uniaxial and biaxial prestrain, respectively.

The dependence of pattern morphology upon the compressive strain (ε_c) was systematically investigated through varying the shape recovery time (t_r) at a fixed recovery temperature of 110 °C. As shown in Figure 2a, the Au film developed a nanoscale wrinkled surface with a random orientation when t_r = 2 s. The contact angle (CA) increased to 102.8° from 89.5° of the smooth surface (Figure S4a,b in

DOI: 10.1021/acsami.8b15535
ACS Appl. Mater. Interfaces 2019, 11, 1563−1570

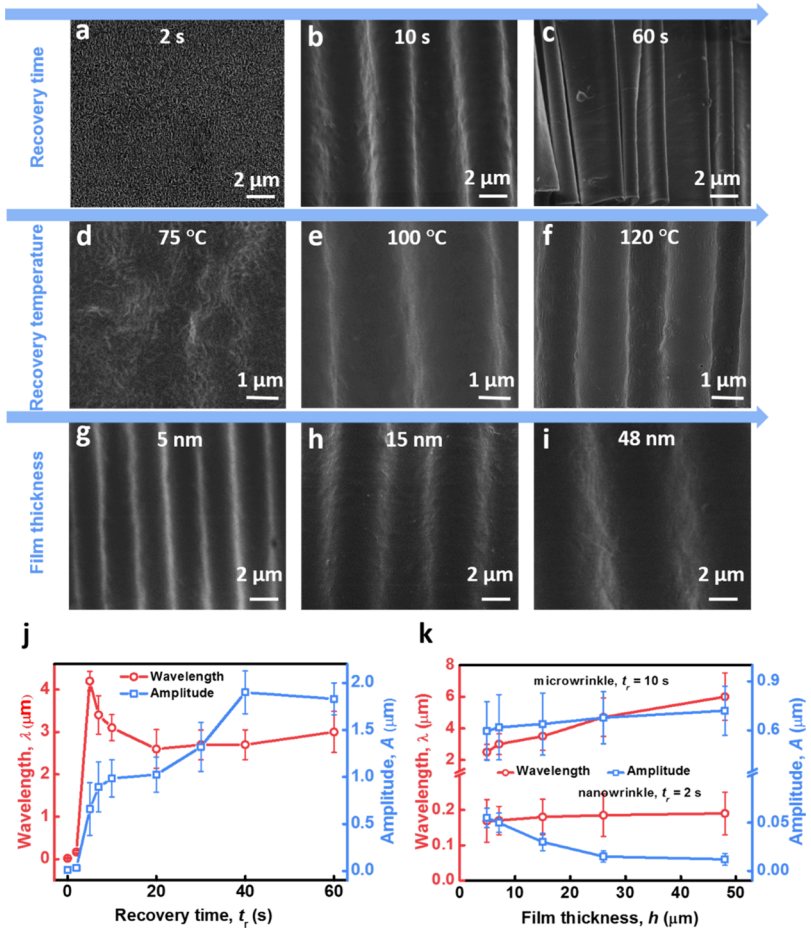

Figure 2. SEM images of the Au film for recovery time (t_r) of 2 (a), 10 (b), 60 s (c), and corresponding wavelength and amplitude of different t_r (j). The thickness of the Au film is ca. 15.0 nm. Effects of recovery temperature (T_r) on the surface morphology: 75 (d), 100 (e), and 120 °C (f). SEM images of patterns with different Au film thickness after recovery for 10 s: 5 (g), 15 (h), 48 nm (i), and the effects of Au film thickness on the wavelength and amplitude (k).

the Supporting Information). When t_r rose to 10 s (a further recovery, larger compressive strain), a periodic and wavy surface was formed (Figure 2b). The wavelength of the feature was ca. 3 μm, and the amplitude was enhanced to 1.0 μm. Therefore, CA of the wrinkled surface sharply increased to 120.3°, as shown in Figure S4c in the Supporting Information. The Au film could be eventually delaminated from the *c*PE substrate after a 60 s shape recovery, (Figure 2c) and the corresponding CA was ca. 128.9° (Figure S4d in the Supporting Information). The increase of CA with the evolution of surface patterns could be utilized for a dynamic control of surface wettability.

Figure 2j demonstrates the wavelength and amplitude of the obtained patterns as a function of t_r. The wavelength of patterns shows a sharp change at t_r of 5 s, due to the transition from nanoscale wrinkles to microscale buckles. The unusual nanoscale wrinkles before the onset of periodic microscale buckles might be related to the discrete feature of the Au film in the nanoscale range (Figure S5 in the Supporting Information). When the Au film was subjected to a small perturbation, interactions between Au nanoparticles might occur to form the nanowrinkles.[48] In this case, continuum theories may break down. However, the Au film can be treated as a continuum membrane when the ε_c is large enough for the formation of microwrinkles. Therefore the linear analysis[49] and nonlinear analysis theory[50,51] can be used for the description of micropatterns of the Au/*c*PE bilayer system. For the bilayer system of Au film/*c*PE, the critical t_r is ca. 5 s. For the bilayer system with large modulus difference (more than 3 orders of magnitude) between two layers, the critical wavelength for the wave-like buckles (microwrinkles) could be approximately written as[52]

$$\lambda_0 \approx 2\pi h\left(\frac{E_f}{E_s}\right)^{1/3} \quad (1)$$

where h is the thickness of the rigid film and E_f and E_s are the modulus of the film and the substrate, respectively. Taking h = 15 nm, $E_f \approx 50$ GPa,[39] $E_s \approx 0.6$ MPa (Figure S1c in the Supporting Information), then λ_0 = 4.1 μm, which is well consistent with the experimental results of ca. 4.2 μm. According to the finite deformation buckling theory,[53] the wavelength of sinusoidal microwrinkle decreases with increasing ε_c and it can be written as

$$\lambda = \frac{\lambda_0(1-\varepsilon_c)}{(1+\xi)^{1/3}} \quad (2)$$

where λ_0 is the wavelength in eq 1 and ξ can be calculated as follows

DOI: 10.1021/acsami.8b15535
ACS Appl. Mater. Interfaces 2019, 11, 1563−1570

$$\xi = \frac{5\varepsilon_c}{32(1-\varepsilon_c)^2} \quad (3)$$

In eq 2, $\lambda_c(1-\varepsilon_c)$ represents the change of wavelength based on simple accordion bellows mechanics and $(1+\xi)^{1/3}$ results from the geometrical nonlinearity and nonlinear constitutive model in the substrate. From eq 3 we can see that ξ depends only on ε_c. According to Figure S3b in the Supporting Information, the ε_c is almost proportional to t_r, and their relation can be written as

$$\varepsilon_c = kt_r \quad (4)$$

where $k = 1.13 \times 10^{-2}$. Combining eqs 2−4 can give rise to the calculated wavelength of sinusoidal microwrinkle, which agrees well with the experimental data (Figure S6 in the Supporting Information). On the other hand, the amplitude of sinusoidal microwrinkle increases monotonically with t_r. We found that a recent work by Wang et al.[54] mentioned the merging of wrinkles in Au/SMP system, while this process does not occur in our system, possibly because of the relatively low t_r here. When t_r continuously increases to 30 and 40 s, the wavelength remains stable, while the amplitude drastically increases with t_r. This is because ridges are formed at this stage, instead of sinusoidal microwrinkle, which could also be confirmed from the scanning electron microscopy (SEM) images (Figure S7 in the Supporting Information). The interfacial delamination occurred after increasing t_r to 60 s. Theoretically, the amplitude of patterns should always increase with the increasing of t_r. However, ultra large ε_c leads to the stacking and collapse of wrinkles (Figure 2c), by which the amplitude declined. These results indicate the surface patterns could be precisely tuned by changing t_r, which lays the foundation for controllably preparing diverse pattern morphologies.

As well as controlling the recovery time, the surface patterns of Au film could also be tuned by changing the recovery temperature (T_r). We compared the resulting surface morphologies at different T_r with the same t_r = 20 s. Increasing T_r can speed up the shape recovery and accordingly enable a higher equivalent compressive strain with given t_r. Therefore, a transition from nanoscale wrinkles to microscale buckles (Figure 2d,e) could also be observed with increased T_r. The pattern amplitudes increase with elevating temperature. Specifically, the amplitude of surface features obtained at 120 °C is ca. 1.8 μm, higher than that (ca. 1.0 μm) obtained at 100 °C. Such observations imply that the recovery temperature is equivalent to above-discussed recovery time regarding controlling the surface morphologies, reminiscent of the time−temperature superposition principle.[54,55] For *c*PE, the shape recovery behavior of a long-time range at low temperature can be extracted from a short-time range behavior at high temperature. For example, we found the pattern obtained with T_r of 120 °C, and t_r of 20 s is similar to the one obtained with T_r of 110 °C and t_r of 40 s.

On the other hand, the morphology of patterns has a strong dependence on the thickness of Au film. For the microscale features formed with t_r of 10 s, a film with increasing thickness has a larger wavelength and amplitude (Figure 2g−i,k), which agrees with the nonlinear analysis of wrinkles in a film bonded to a compliant substrate.[50] The nanoscale features formed with t_r of 2 s are randomly oriented. For quantitative description of the nanowrinkles, we defined the wavelength as the average distance between the wrinkles and the feature size as the average length of wrinkles. We found the wavelength changes little while the amplitude and feature size decrease with film thickness (Figures S8, 2k, and S9 in the Supporting Information). The nonlinear analysis cannot explain these nanoscale features, suggesting that the discrete nanostructures need to be considered for analysis. To sum up, the adoption of SMP-based substrate provides versatile manners in controllably tuning the pattern morphology, which is the basis for preparing more complex patterns in a designable way.

To further extend this methodology for creating superimposed complex patterns, the prestrain could be applied biaxially, followed by a simultaneous or sequential release of the prestrain. For the simultaneous release of biaxial strain, the anisotropy of patterns could be tuned by controlling the initial prestrain of the orthogonal axis. The two orthogonal compressive strain in the SMP substrate in the xand y directions are defined as ε_x and ε_y, respectively (Figure S10a in the Supporting Information). Our observed pattern can be well captured by the numerical simulations built on Fourier spectral method (Figure S10d−i in the Supporting Information). Notably, when the prestrain is the same for the orthogonal axis, homogeneous and isotropic microscale wrinkles could be prepared (Figure 3a). However, a sequential strain release could be achieved by releasing ε_x during the first shape recovery process, followed by a release of ε_y through the second shape recovery. The sequential strain release renders a different morphology even with the same total recovered strain, with the wavelength of primarily formed buckles lower than buckles formed afterward (Figure 3b). According to our simulation results, we attribute such behavior to the changed

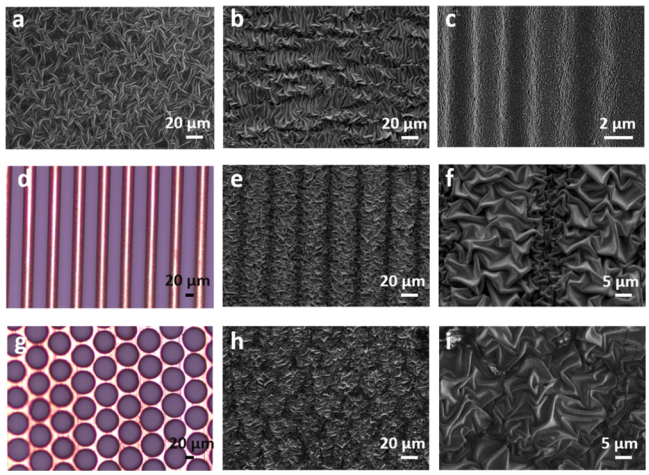

Figure 3. Preparation of multiscale complex patterns. (a) SEM image of patterned surface with the biaxial strain simultaneously released. (b) SEM image of patterned surface with the biaxial strain sequentially released, the compressive strain of two directions are ca. 33% for (a,b). (c) SEM image of surface patterns after two-step shape recovery process, with the t_{r1} = 2 s and the t_{r2} = 10 s. (d) Hollowed copper plate template with rectangular voids. The width of the rectangular voids is ca. 35 μm, and the distance between the voids is ca. 25 μm. (e) SEM image of the Au film after predefining the film with template (d) and biaxial shape recovery of the substrate. (f) Magnified view of (e). (g) Hollowed copper plate template with circular voids. The diameter of the circular voids is ca. 55 μm and the distance between voids is ca. 5 μm. (h) SEM image of Au film after predefining the film with template (g) and biaxial shape recovery of the substrate. (i) Magnified view of (h).

DOI: 10.1021/acsami.8b15535
ACS Appl. Mater. Interfaces 2019, 11, 1563−1570

equivalent film thickness after the formation of primary buckles.

Multiscale hierarchical surface patterns could also be prepared by sequential prestrain release along the same axis. As a representative case, a hierarchical surface with microscale wave-like buckles and nanoscale random wrinkles could be obtained (Figure 3c), through a two-step shape recovery process (t_{r1} = 2 s, t_{r2} = 10 s). The small nanowrinkles are formed because of the same reason as we discussed above. For the second shape recovery process, the Au/*c*PE system develops microwrinkles on the basis of the nanowrinkles, leading to multiscale hierarchical surface patterns. On the other hand, the patterns of Au film could be enriched by predefining the shape of film in the deposition process, through the usage of shadow masks. Representatively, copper plates with rectangular (Figure 3d) and circular (Figure 3g) voids are applied for spatially defined Au deposition. We found that there was still Au element in the covered area although it was significantly less than that of the uncovered region (Figure S11 in the Supporting Information). After a biaxial shape recovery process, the pattern morphology for the uncovered and covered region showed a dramatic difference. The wrinkles of uncovered area demonstrated increased wavelength and amplitude, compared with the wrinkles in the masked area, which could be attributed to a higher film thickness in the uncovered region (Figure 3e,f,h,i). We also increased the space to ca. 50 μm between the uncovered areas, which exhibited a similar phenomenon after recovery (Figure S12 in the Supporting Information). The combination of spatial predefining and shape recovery-induced wrinkle formation provides a scalable way for creating superimposed surface patterns.

For a traditional bilayer system, spatially defined formation of patterns can hardly be achieved because the strain distribution amongst the film is nearly homogeneous. The strain distribution of Au/*c*PE system is also uniform without the heat stimuli (Figure S13 in the Supporting Information). However, the release of prestrain for our SMP-based substrate lies in heat profiles of this system, which can be both homogeneously and inhomogeneously controlled. To this end, we exploit a focused laser beam to locally activate the patterning of the Au film. For a simplified case, a round laser spot is concentrated on the sputtered Au film (the inset of Figure 4a). Laser illumination could dramatically raise the local temperature and thus induced the shape recovery process within the laser spot. When the bilayer system was irradiated by a laser beam with 1 W power for 20 s, the local wrinkle was formed, as shown in Figure 4a. We found that the center of the wrinkle is random and the edge is radially oriented, which is due to the temperature gradient from the center to the periphery of the laser spot. The temperature within the laser spot increased with the laser power, as well as illumination time (Figure S14 in the Supporting Information). The highest temperatures of different power laser (1, 2, and 3 W) were 102, 125, and 148 °C, respectively, with 20 s radiation. The corresponding wavelengths of obtained features were 6.5, 5.8, and 3.6 μm, respectively (Figure S15 in the Supporting Information). These values were larger than the features obtained at 100 °C (Figure 2e, wavelength ca. 2.9 μm) and 120 °C (Figure 2f, wavelength ca. 2.3 μm) with the overall heating way, which resulted in a free recovery process. The higher wavelength could be explained by the reduced ε_c compared with the overall heating method because of the restraint of the unradiated areas.

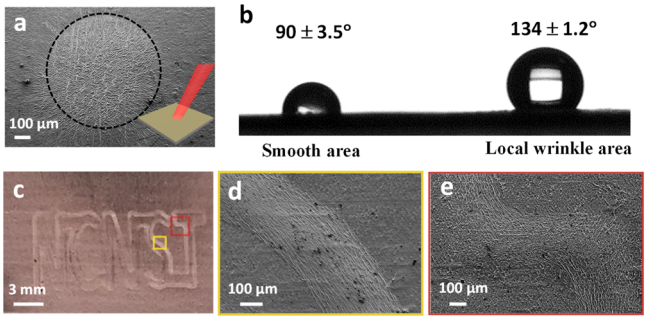

Figure 4. Preparation of spatially confined surface patterns. (a) SEM image of *c*PE/Au bilayer after being illuminated by a laser beam with a round spot. The laser power is 1 W. Inset: The schematic of the laser-induced local heating process. (b) CA of smooth surface and laser-induced wrinkled surface. (c) Acronym "NCNST" written on the *c*PE-supported Au film by a focus laser "pencil". The zoomed-in view of regions in colored box is shown in (d,e), respectively.

We prepared the wrinkled surface within the illuminated region and kept the left regions smooth. The difference of CA between patterned and smooth region also validates the potential of this methodology for selective surface functionalization (Figure 4b). The morphology of patterns could also be controlled by changing the laser power, which directly determines the local temperature. The laser beam could be further used as a "pencil" to "write" an arbitrary pattern (e.g., NCNST, short for National Center for Nanoscience and Technology) on the Au film, with the illuminated region wrinkled along the track of the laser beam (Figure 4c,d,e). The capability of local patterning was typically prohibited in the bilayer system by traditional thermostable substrates, further highlighting the advantages by using SMPs to construct surface patterns.

To explore the application of the patterned surface, we constructed a piezoresistive pressure sensor by laminating two patterned films face-to-face. Pressures perpendicular to the contact interface could increase the contact area between two films, and the electrical current would increase accordingly when a drain voltage is applied. As shown in Figure 5b, a rectangular wave of applied pressures could generate a quick and sharp response in electrical current. The sensitivity of the pressure sensor is defined as

$$S = (\Delta I/I_0)/P \quad (5)$$

where ΔI is the change in device current, I_0 is the original device current, and P is the applied pressure. The as-prepared pressure sensor exhibited a high sensitivity of 15 kPa^{-1} below 0.3 kPa, and 1 kPa^{-1} below 4 kPa (Figure 5c), which is comparable to state-of-the-art piezoresistive pressure sensors.[56−60] The performance of piezoresistive pressure sensors is determined by the contact between protuberances of the overlapped film, which is directly related to the density and morphology of surface patterns.[13,61,62] For the pressure sensor constructed by smooth films, the performance is far inferior in terms of sensitivity and operational range (Figure S16a in the Supporting Information). The patterned film-based pressure sensor was capable of detecting both small pressures and vibrations sensitively and recording the variation of pressures reliably with a high-pressure range. Besides, the pressure sensor demonstrated outstanding stability under cyclic tests (Figure S16c in the Supporting Information).

DOI: 10.1021/acsami.8b15535
ACS Appl. Mater. Interfaces 2019, 11, 1563−1570

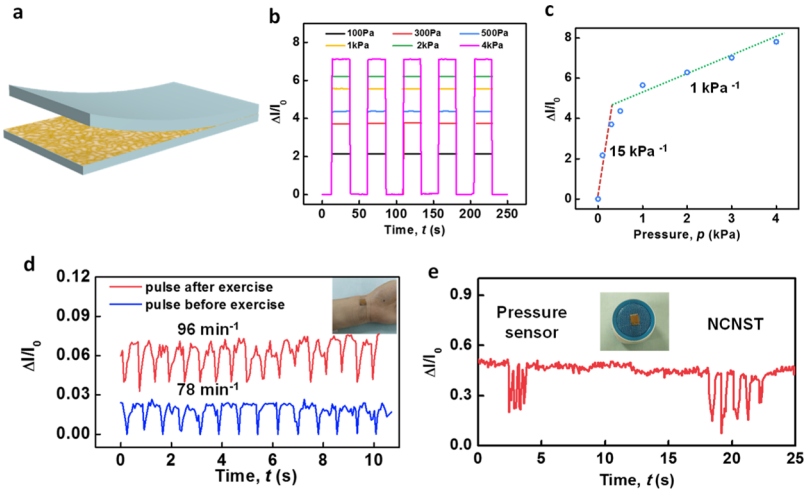

Figure 5. Application of the patterned surface as a piezoresistive pressure sensor. (a) Schematic of the pressure sensor. (b) Response in electrical current under different applied pressure. (c) Sensitivity of the pressure sensor within the range 0−4 kPa. (d) Application of the pressure sensor for the sensing of the wrist pulse. Inset: The pressure sensor attached onto the wrist. (e) Application of the pressure sensor for sound sensing, with a different form of wavepacket upon different phrases broadcasted by a sound box. Inset: The pressure sensor attached to a loudspeaker of a sound box.

The pressure sensor could be applied for sensitive detection of the wrist pulse (Figure 5d), as well as differentiate the acoustic vibration of different phrases (Figure 5e), showing great promise in electronic skin applications.

CONCLUSIONS

In summary, we developed a facile method for preparing surface patterns by using the instability of bilayer system. Through the adoption of SMPs as the flexible substrates, the morphology of patterns could be tuned through various manners, including changing the shape recovery temperature and time of the SMP-based substrate, as well as controlling the thickness of Au film. Complex surface patterns could be prepared by biaxial shape recovery, sequential shape recovery, and predefining the Au film using a shadow mask. In addition, the patterns could be spatially localized within the film through laser-induced local heating, which could hardly be achieved by the non-SMP substrate. The patterned surface could be constructed into a piezoresistive pressure sensor, which demonstrated high sensitivity and operational range and could be applied for the detection of pulse and sounds. The SMP-based substrates demonstrate unique advantages in constructing bilayer systems for surface patterning, which have great promise in the preparation of smart surfaces.

EXPERIMENTAL SECTION

Materials. PE (type Vestenamer 8012) pellets bought from Evonik Industries AG (Germany) have a density of 0.910 g cm^{-3} and a melt flow index of 16 g $(10\ min)^{-1}$. Initiator DHBP (97% purity) was purchased from Beijing J&K Chemical Company, China.

Sample Preparations. First, PE pellets were melted in a mixer (HAAKE Rheomix 3010 OS, Germany) under 120 °C for 5 min. The stirring speed was set as 50 rpm. Then, DHBP was added to the melted PE and mixed under stirring for 10 min to make it dispersed uniformly. Then, they were compressed via a hot press machine (Qien, R-3221, China) at 180 °C under 20 MPa for 10 min to get thin films with thickness of 0.2−0.5 mm. The stretched uniaxial samples with ca. 200% prestrain were obtained at ca. 110.0 °C by a tensile hot stage (Linkam TST350, UK) and then fixed the deformation by cooling to the room temperature. The biaxially stretched samples were obtained by a tailor-made biaxial drawing instrument at 110.0 °C and then cooling to the room temperature. The Au film was coated on the stretched sample via a vacuum sputtering coater (Denton Desk IV, USA) for 15−240 s. The local wrinkle was obtained by a diode laser system (BWT Beijing LTD, China) with the center wavelength of 808 nm. The letter was written by a laser cutting machine (Chutian laser group CT-LEG50, China) with a radiation power of 3.5 W and speed of 12 mm s^{-1}.

Property Characterizations. The morphology observation of the samples was carried out on SEM (NOVA Nano N-430, USA) running at an accelerating voltage of 5 kV and an optical microscope (Leica DM4100, Germany). The atomic force microscopy images were taken with Digital Instruments (Bruker 3100, Germany) in tapping mode. CAs were measured by an equipment (Kruss DSA 100, Germany) at different positions five times, corresponding to 3 μL of distilled water droplets, respectively.

Pressure Sensor Fabrication and Pressure Sensing Test. The pressure sensor is composed of two layers of patterned *c*PE/Au (10 mm × 10 mm) face-to-face overlapped, with silver wires attached onto one end of each film. The pressures are applied by a dynamic mechanical thermal analyzer (DMTA) (TA Q800, USA), and the current is recorded in situ by a semiconductor parameter analyzer (Tektronix Keithley 4200-SCS, USA). For the sensing of wrist pulse and sounds, the pressure sensor is adhered onto a wrist or loudspeaker by an adhesive tape.

ASSOCIATED CONTENT

Supporting Information

The Supporting Information is available free of charge on the ACS Publications website at DOI: 10.1021/acsami.8b15535.

Mechanical property and shape memory cycle, effective of temperature and time, Au film thickness, and simulated results are given in Figures S1−S16 (PDF)

AUTHOR INFORMATION

Corresponding Authors

*E-mail: zhaoj@nanoctr.cn (J.Z.).
*E-mail: zhong.zhang@nanoctr.cn (Z.Z.).

ORCID

Zhaohe Dai: 0000-0002-5205-089X
Jin Zhang: 0000-0003-3731-8859
Zhong Zhang: 0000-0002-9102-1311

DOI: 10.1021/acsami.8b15535
ACS Appl. Mater. Interfaces 2019, 11, 1563−1570

Notes

The authors declare no competing financial interest.

■ ACKNOWLEDGMENTS

This work was financially supported by the National Natural Science Foundation of China (grant nos. 11832010 and 11225210).

■ REFERENCES

(1) Liu, K.; Jiang, L. Bio-inspired design of multiscale structures for function integration. *Nano Today* **2011**, *6*, 155−175.
(2) Guo, H.-Y.; Li, Q.; Zhao, H.-P.; Zhou, K.; Feng, X.-Q. Functional Map of Biological and Biomimetic Materials with Hierarchical Surface Structures. *RSC Adv.* **2015**, *5*, 66901−66926.
(3) Barthlott, W.; Neinhuis, C. Purity of the Sacred Lotus, or Escape from Contamination in Biological Surfaces. *Planta* **1997**, *202*, 1−8.
(4) Geim, A. K.; Dubonos, S. V.; Grigorieva, I. V.; Novoselov, K. S.; Zhukov, A. A.; Shapoval, S. Y. Microfabricated Adhesive Mimicking Gecko Foot-Hair. *Nat. Mater.* **2003**, *2*, 461−463.
(5) Xu, H.; Yu, C.; Wang, S.; Malyarchuk, V.; Xie, T.; Rogers, J. A. Deformable, Programmable, and Shape-Memorizing Micro-Optics. *Adv. Funct. Mater.* **2013**, *23*, 3299−3306.
(6) Kim, B. H.; Onses, M. S.; Lim, J. B.; Nam, S.; Oh, N.; Kim, H.; Yu, K. J.; Lee, J. W.; Kim, J.-H.; Kang, S.-K.; Lee, C. H.; Lee, J.; Shin, J. H.; Kim, N. H.; Leal, C.; Shim, M.; Rogers, J. A. High-Resolution Patterns of Quantum Dots Formed by Electrohydrodynamic Jet Printing for Light-Emitting Diodes. *Nano Lett.* **2015**, *15*, 969−973.
(7) Luan, B.; Robbins, M. O. The Breakdown of Continuum Models for Mechanical Contacts. *Nature* **2005**, *435*, 929−932.
(8) Tian, Y.; Jiang, L. Intrinsically robust hydrophobicity. *Nat. Mater.* **2013**, *12*, 291−292.
(9) Feng, X.; Feng, L.; Jin, M.; Zhai, J.; Jiang, L.; Zhu, D. Reversible Super-hydrophobicity to Super-hydrophilicity Transition of Aligned ZnO Nanorod Films. *J. Am. Chem. Soc.* **2004**, *126*, 62−63.
(10) Zhao, L.; Zhao, J.; Liu, Y.; Guo, Y.; Zhang, L.; Chen, Z.; Zhang, H.; Zhang, Z. Continuously Tunable Wettability by Using Surface Patterned Shape Memory Polymers with Giant Deformability. *Small* **2016**, *12*, 3327−3333.
(11) Ohzono, T.; Monobe, H.; Shiokawa, K.; Fujiwara, M.; Shimizu, Y. Shaping Liquid on a Micrometre Scale Using Microwrinkles as Deformable Open Channel Capillaries. *Soft Matter* **2009**, *5*, 4658−4664.
(12) Thomas, A. V.; Andow, B. C.; Suresh, S.; Eksik, O.; Yin, J.; Dyson, A. H.; Koratkar, N. Controlled Crumpling of Graphene Oxide Films for Tunable Optical Transmittance. *Adv. Mater.* **2015**, *27*, 3256−3265.
(13) Shi, J.; Wang, L.; Dai, Z.; Zhao, L.; Du, M.; Li, H.; Fang, Y. Multiscale Hierarchical Design of a Flexible Piezoresistive Pressure Sensor with High Sensitivity and Wide Linearity Range. *Small* **2018**, *14*, 1800819.
(14) Wei, Y.; Chen, S.; Lin, Y.; Yang, Z.; Liu, L. Cu-Ag Core-Shell Nanowires for Electronic Skin with a Petal Molded Microstructure. *J. Mater. Chem. C* **2015**, *3*, 9594−9602.
(15) Liu, Z.; Wang, X.; Qi, D.; Xu, C.; Yu, J.; Liu, Y.; Jiang, Y.; Liedberg, B.; Chen, X. High-Adhesion Stretchable Electrodes Based on Nanopile Interlocking. *Adv. Mater.* **2016**, *29*, 1603382.
(16) Liu, J.; Fu, T.-M.; Cheng, Z.; Hong, G.; Zhou, T.; Jin, L.; Duvvuri, M.; Jiang, Z.; Kruskal, P.; Xie, C.; Suo, Z.; Fang, Y.; Lieber, C. M. Syringe-Injectable Electronics. *Nat. Nanotechnol.* **2015**, *10*, 629−636.
(17) Viventi, J.; Kim, D.-H.; Vigeland, L.; Frechette, E. S.; Blanco, J. A.; Kim, Y.-S.; Avrin, A. E.; Tiruvadi, V. R.; Hwang, S.-W.; Vanleer, A. C.; Wulsin, D. F.; Davis, K.; Gelber, C. E.; Palmer, L.; Van der Spiegel, J.; Wu, J.; Xiao, J.; Huang, Y.; Contreras, D.; Rogers, J. A.; Litt, B. Flexible, Foldable, Actively Multiplexed, High-Density Electrode Array for Mapping Brain Activity in Vivo. *Nat. Neurosci.* **2011**, *14*, 1599−1605.
(18) Wang, Y.; Sun, Q.; Xiao, J. Simultaneous Formation of Multiscale Hierarchical Surface Morphologies through Sequential Wrinkling and Folding. *Appl. Phys. Lett.* **2018**, *112*, 081602.
(19) Huck, W. T. S.; Bowden, N.; Onck, P.; Pardoen, T.; Hutchinson, J. W.; Whitesides, G. M. Ordering of Spontaneously Formed Buckles on Planar Surfaces. *Langmuir* **2000**, *16*, 3497−3501.
(20) Zang, J.; Ryu, S.; Pugno, N.; Wang, Q.; Tu, Q.; Buehler, M. J.; Zhao, X. Multifunctionality and Control of the Crumpling and Unfolding of Large-Area Graphene. *Nat. Mater.* **2013**, *12*, 321−325.
(21) Yu, S.; Sun, Y.; Ni, Y.; Zhang, X.; Zhou, H. Controlled Formation of Surface Patterns in Metal Films Deposited on Elasticity-Gradient PDMS Substrates. *ACS Appl. Mater. Interfaces* **2016**, *8*, 5706−5714.
(22) Bowden, N.; Brittain, S.; Evans, A. G.; Hutchinson, J.W.; Whitesides, G. M. Spontaneous Formation of Ordered Structures in Thin Films of Metals Supported on an Elastomeric Polymer. *Nature* **1998**, *393*, 146−149.
(23) Ding, W.; Yang, Y.; Zhao, Y.; Jiang, S.; Cao, Y.; Lu, C. Well-Defined Orthogonal Surface Wrinkles Directed by the Wrinkled Boundary. *Soft Matter* **2013**, *9*, 3720−3726.
(24) Jeong, H.-C.; Park, H.-G.; Lee, J. H.; Seo, D.-S. Localized Ion-Beam Irradiation-Induced Wrinkle Patterns. *ACS Appl. Mater. Interfaces* **2015**, *7*, 23216−23222.
(25) Li, F.; Hou, H.; Yin, J.; Jiang, X. Near-infrared light-responsive dynamic wrinkle patterns. *Sci. Adv.* **2018**, *4*, No. eaar5762.
(26) Jiang, T.; Huang, R.; Zhu, Y. Interfacial Sliding and Buckling of Monolayer Graphene on a Stretchable Substrate. *Adv. Funct. Mater.* **2013**, *24*, 396−402.
(27) Mather, P. T.; Luo, X.; Rousseau, I. A. Shape Memory Polymer Research. *Annu. Rev. Mater. Res.* **2009**, *39*, 445−471.
(28) Xie, T. Tunable Polymer Multi-Shape Memory Effect. *Nature* **2010**, *464*, 267−270.
(29) Leng, J.; Lv, H.; Liu, Y.; Du, S. Electroactivate Shape-Memory Polymer Filled with Nanocarbon Particles and Short Carbon Fibers. *Appl. Phys. Lett.* **2007**, *91*, 144105.
(30) Lendlein, A.; Jiang, H.; Jünger, O.; Langer, R. Light-Induced Shape-Memory Polymers. *Nature* **2005**, *434*, 879−882.
(31) Huang, M.; Dong, X.; Wang, L.; Zhao, J.; Liu, G.; Wang, D. Two-way shape memory property and its structural origin of cross-linked poly(ε-caprolactone). *RSC Adv.* **2014**, *4*, 55483−55494.
(32) Fang, Z.; Zheng, N.; Zhao, Q.; Xie, T. Healable, Reconfigurable, Reprocessable Thermoset Shape Memory Polymer with Highly Tunable Topological Rearrangement Kinetics. *ACS Appl. Mater. Interfaces* **2017**, *9*, 22077−22082.
(33) Leng, J.; Lan, X.; Liu, Y.; Du, S. Shape-memory polymers and their composites: Stimulus methods and applications. *Prog. Mater. Sci.* **2011**, *56*, 1077−1135.
(34) Kuang, X.; Liu, G.; Dong, X.; Wang, D. Triple-Shape Memory Epoxy Based on Diels-Alder Adduct Molecular Switch. *Polymer* **2016**, *84*, 1−9.
(35) Fu, C.-C.; Grimes, A.; Long, M.; Ferri, C. G. L.; Rich, B. D.; Ghosh, S.; Ghosh, S.; Lee, L. P.; Gopinathan, A.; Khine, M. Tunable Nanowrinkles on Shape Memory Polymer Sheets. *Adv. Mater.* **2010**, *21*, 4472−4476.
(36) Li, J.; An, Y.; Huang, R.; Jiang, H.; Xie, T. Unique Aspects of a Shape Memory Polymer as the Substrate for Surface Wrinkling. *ACS Appl. Mater. Interfaces* **2012**, *4*, 598−603.
(37) Gabardo, C. M.; Yang, J.; Smith, N. J.; Adams-McGavin, R. C.; Soleymani, L. Programmable Wrinkling of Self-Assembled Nanoparticle Films on Shape Memory Polymers. *ACS Nano* **2016**, *10*, 8829−8836.
(38) Zhao, Y.; Huang, W. M.; Fu, Y. Q. Formation of Micro/Nano-Scale Wrinkling Patterns atop Shape Memory Polymers. *J. Micromech. Microeng.* **2011**, *21*, 067007.
(39) Schauer, S.; Worgull, M.; Hölscher, H. Bio-Inspired Hierarchical Micro- and Nano-Wrinkles Obtained via Mechanically Directed Self-Assembly on Shape-Memory Polymers. *Soft Matter* **2017**, *13*, 4328−4334.

DOI: 10.1021/acsami.8b15535
ACS Appl. Mater. Interfaces 2019, 11, 1563−1570

(40) Chen, Z.; Young, K. Y.; Krishnaswamy, S. Anisotropic Wrinkle Formation on Shape Memory Polymer Substrates. *J. Appl. Phys.* **2012**, *112*, 124319.
(41) Lee, W.-K.; Engel, C. J.; Huntington, M. D.; Hu, J.; Odom, T. W. Controlled Three-Dimensional Hierarchical Structuring by Memory-Based, Sequential Wrinkling. *Nano Lett.* **2015**, *15*, 5624−5629.
(42) Chen, P.-Y.; Sodhi, J.; Qiu, Y.; Valentin, T. M.; Steinberg, R. S.; Wang, Z.; Hurt, R. H.; Wong, I. Y. Multiscale Graphene Topographies Programmed by Sequential Mechanical Deformation. *Adv. Mater.* **2016**, *28*, 3564−3571.
(43) Xie, T.; Xiao, X.; Li, J.; Wang, R. Encoding Localized Strain History through Wrinkle Based Structural Colors. *Adv. Mater.* **2010**, *22*, 4390−4394.
(44) Wang, M. C.; Chun, S.; Han, R. S.; Ashraf, A.; Kang, P.; Nam, S. Heterogeneous, Three-Dimensional Texturing of Graphene. *Nano Lett.* **2015**, *15*, 1829−1835.
(45) Zhao, J.; Chen, M.; Wang, X.; Zhao, X.; Wang, Z.; Dang, Z.-M.; Ma, L.; Hu, G.-H.; Chen, F. Triple Shape Memory Effects of Cross-Linked Polyethylene/Polypropylene Blends with Cocontinuous Architecture. *ACS Appl. Mater. Interfaces* **2013**, *5*, 5550−5556.
(46) Wang, Z.; Zhao, J.; Chen, M.; Yang, M.; Tang, L.; Dang, Z.-M.; Chen, F.; Huang, M.; Dong, X. Dually Actuated Triple Shape Memory Polymers of Cross-Linked Polycyclooctene-Carbon Nanotube/Polyethylene Nanocomposites. *ACS Appl. Mater. Interfaces* **2014**, *6*, 20051−20059.
(47) Ma, L.; Zhao, J.; Wang, X.; Chen, M.; Liang, Y.; Wang, Z.; Yu, Z.; Hedden, R. C. Effects of Carbon Black Nanoparticles on Two-Way Reversible Shape Memory in Crosslinked Polyethylene. *Polymer* **2015**, *56*, 490−497.
(48) Leahy, B. D.; Pocivavsek, L.; Meron, M.; Lam, K. L.; Salas, D.; Viccaro, P. J.; Lee, K. Y. C.; Lin, B. Geometric Stability and Elastic Response of a Supported Nanoparticle Film. *Phys. Rev. Lett.* **2010**, *105*, 058301.
(49) Niu, K.; Talreja, R. Modeling of Wrinkling in Sandwich Panels under Compression. *J. Eng. Mech.* **1999**, *125*, 875−883.
(50) Huang, Z. Y.; Hong, W.; Suo, Z. Nonlinear Analyses of Wrinkles in a Film Bonded to a Compliant Substrate. *J. Mech. Phys. Solid.* **2005**, *53*, 2101−2118.
(51) Huang, R. Kinetic wrinkling of an elastic film on a viscoelastic substrate. *J. Mech. Phys. Solid.* **2005**, *53*, 63−89.
(52) Wang, Q.; Zhao, X. Beyond Wrinkles: Multimodal Surface Instabilities for Multifunctional Patterning. *MRS Bull.* **2016**, *41*, 115−122.
(53) Jiang, H.; Khang, D.-Y.; Song, J.; Sun, Y.; Huang, Y.; Rogers, J. A. Finite Deformation Mechanics in Buckled Thin Films on Compliant Supports. *Proc. Natl. Acad. Sci. U.S.A.* **2007**, *104*, 15607−15612.
(54) Wang, Y.; Yu, K.; Qi, H. J.; Xiao, J. Temperature Dependent Evolution of Wrinkled Single-Crystal Silicon Ribbons on Shape Memory Polymers. *Soft Matter* **2017**, *13*, 7625−7632.
(55) Yu, K.; Ge, Q.; Qi, H. J. Reduced Time as a Unified Parameter Determining Fixity and Free Recovery of Shape Memory Polymers. *Nat. Commun.* **2014**, *5*, 3066.
(56) Su, B.; Gong, S.; Ma, Z.; Yap, L. W.; Cheng, W. Mimosa-Inspired Design of A Flexible Pressure Sensor with Touch Sensitivity. *Small* **2014**, *11*, 1886−1891.
(57) Jian, M.; Xia, K.; Wang, Q.; Yin, Z.; Wang, H.; Wang, C.; Xie, H.; Zhang, M.; Zhang, Y. Flexible and Highly Sensitive Pressure Sensors Based on Bionic Hierarchical Structures. *Adv. Funct. Mater.* **2017**, *27*, 1606066.
(58) Kim, K.-H.; Hong, S. K.; Jang, N.-S.; Ha, S.-H.; Lee, H. W.; Kim, J.-M. Wearable Resistive Pressure Sensor Based on Highly Flexible Carbon Composite Conductors with Irregular Surface Morphology. *ACS Appl. Mater. Interfaces* **2017**, *9*, 17499−17507.
(59) Chen, W.; Gui, X.; Liang, B.; Yang, R.; Zheng, Y.; Zhao, C.; Li, X.; Zhu, H.; Tang, Z. Structural Engineering for High Sensitivity, Ultrathin Pressure Sensors Based on Wrinkled Graphene and Anodic Aluminum Oxide Membrane. *ACS Appl. Mater. Interfaces* **2017**, *9*, 24111−24117.
(60) Wang, X.; Gu, Y.; Xiong, Z.; Cui, Z.; Zhang, T. Silk-Molded Flexible, Ultrasensitive, and Highly Stable Electronic Skin for Monitoring Human Physiological Signals. *Adv. Mater.* **2013**, *26*, 1336−1342.
(61) Bae, G. Y.; Pak, S. W.; Kim, D.; Lee, G.; Kim, D. H.; Chung, Y.; Cho, K. Linearly and Highly Pressure-Sensitive Electronic Skin Based on a Bioinspired Hierarchical Structural Array. *Adv. Mater.* **2016**, *28*, 5300−5306.
(62) Shu, Y.; Tian, H.; Yang, Y.; Li, C.; Cui, Y.; Mi, W.; Li, Y.; Wang, Z.; Deng, N.; Peng, B.; Ren, T.-L. Surface-modified Piezoresistive Nanocomposite Flexible Pressure Sensors with High Sensitivity and Wide Linearity. *Nanoscale* **2015**, *7*, 8636−8644.

DOI: 10.1021/acsami.8b15535
ACS Appl. Mater. Interfaces 2019, 11, 1563−1570